MYCOLOGY
2025, VOL. 16, NO. 2, 941–955
https://doi.org/10.1080/21501203.2024.2426484

Taylor & Francis
Taylor & Francis Group

RESEARCH ARTICLE

OPEN ACCESS Check for updates

Improving the production of micafungin precursor FR901379 in *Coleophoma empetri* using heavy-ion irradiation and its mechanism analysis

Yongjuan Liu[a,b,c*], Beibei Wang[a,b,c*], Xiaoxi Zhang[a,b,c], Ping Men[a,b,c], Meng Gu[a,b,c,d], Yu Zhou[a,b,c,e], Wei Hu[d,f], Zhuanzi Wang[f], Min Wang[a,b,c], Xuenian Huang[a,b,c,d] and Xuefeng Lu[a,b,c,d,g,h]

[a]Shandong Provincial Key Laboratory of Synthetic Biology, Qingdao Institute of Bioenergy and Bioprocess Technology, Chinese Academy of Sciences, Qingdao, China; [b]Shandong Energy Institute, Qingdao, China; [c]Qingdao New Energy Shandong Laboratory, Qingdao, China; [d]University of Chinese Academy of Sciences, Beijing, China; [e]Institute for Smart Materials & Engineering, University of Jinan, Jinan, China; [f]Institute of Modern Physics Chinese Academy of Sciences, Lanzhou, China; [g]Key Laboratory of Biofuels, Qingdao Institute of Bioenergy and Bioprocess Technology, Chinese Academy of Sciences, Qingdao, China; [h]Marine Biology and Biotechnology Laboratory, Qingdao National Laboratory for Marine Science and Technology, Qingdao, China

ABSTRACT

Micafungin is a semisynthetic echinocandin antifungal agent derived from fungal natural product FR901379 produced by *Coleophoma empetri*, facing challenges in biomanufacturing due to poor chassis performance and unclear high-yield mechanisms. In this study, the mutagenic effects of heavy-ion beam and how fungi repaired damage show that compared to the wild-type strain, nonhomologous end-joining pathway deficient mutants were more sensitive to heavy ion radiation, resulting in higher lethality rates and more mutations from the same radiation dose. Moreover, mutants obtained through two rounds of heavy-ion irradiation mutagenesis produced 1.1 g/L of FR901379, representing a remarkable increase of 253.7%. Compared to the parent strain, the mutants displayed noticeable differences in morphology and fermentation status. Comparative genomic analysis revealed mutations in several genes critical for morphological differentiation, which may have enhanced the production of FR901379 in the excellent mutants. This study has implications for the application of heavy-ion irradiation to filamentous fungi breeding. Additionally, the mutants with high FR901379 titre not only improve the production efficiency of micafungin but also provide a better chassis and theoretical guidance for subsequent metabolic engineering.

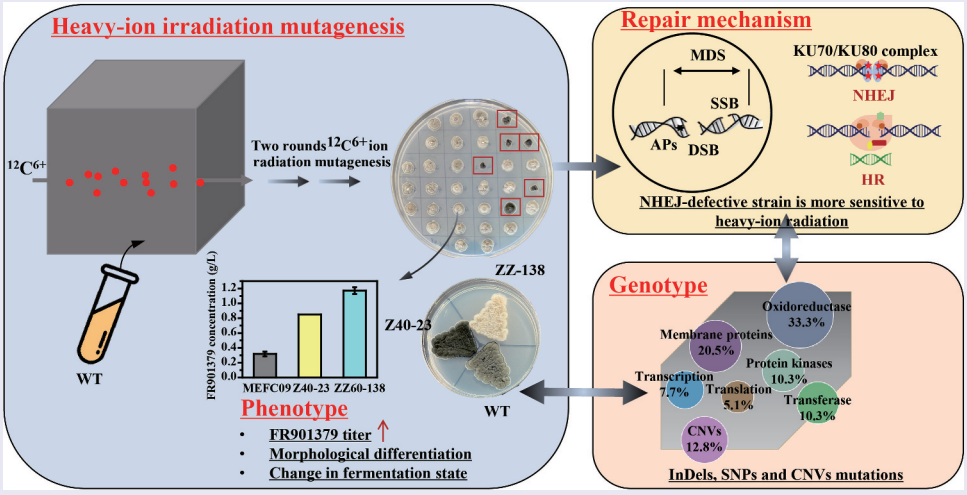

ARTICLE HISTORY
Received 23 July 2024
Accepted 4 November 2024

KEYWORDS
Micafungin; *Coleophoma empetri*; heavy-ion irradiation; nonhomologous end-joining; high-yield mechanism

CONTACT Xuenian Huang huangxn@qibebt.ac.cn; Xuefeng Lu lvxf@qibebt.ac.cn Shandong Provincial Key Laboratory of Synthetic Biology, Qingdao Institute of Bioenergy and Bioprocess Technology, Chinese Academy of Sciences, Qingdao 266101, China
*These authors contributed equally to this work.

Supplemental data for this article can be accessed online at https://doi.org/10.1080/21501203.2024.2426484

1. Introduction

Echinocandins are nonribosomal cyclic hexapeptides conjugated with a fatty acid or highly reduced polyketide side chain, synthesised by filamentous fungi (Denning 2003; Emri et al. 2013). They are a new type of antifungal drugs that inhibit the activity of β-1,3-glucan synthase and interfere with the synthesis of fungal cell walls, including caspofungin, micafungin, anidulafungin, and razafungin. Due to their broad antimicrobial spectrum and high safety profile, echinocandins have become first-line therapies for treating invasive fungal infections (Szymański et al. 2022). Unlike the other echinocandins, micafungin displays exceptional water solubility due to its sulphonate group, a rare feature in natural compounds (Iwamoto 1994). The presence of the sulphonate group can provide drugs with distinct pharmacological properties, thereby enhancing their bioavailability (Hashimoto 2009). Therefore, micafungin has garnered significant attention in the field of drug research, establishing its value among enterprises.

In industry, micafungin is chemically synthesised from FR901379 which is a natural product produced by *Coleophoma empetri* (Hashimoto 1994; Tomishima et al. 2008a, 2008b). Therefore, the production of FR901379 is the key step in the manufacture of micafungin, a natural FR901379 producer isolated from soil like other organisms, exhibits a limited ability to biosynthesize the desired metabolite (Kanda et al. 2009; Ueda et al. 2011). Thus, enhancing the synthesis capability of *C. empetri* to produce FR901379 emerges as a viable approach to minimise production costs. Metabolic engineering modifications targeting core pathways have been widely employed in genetic breeding, with a comprehensive understanding of biosynthetic mechanisms constituting a crucial prerequisite. In previous studies, researchers from our lab have identified the core biosynthetic pathway and sulphonate group through gene knockout and heterologous expression (Men et al. 2022). Then, the titre of FR901379 was increased from 0.3 g/L to 1.3 g/L by metabolic engineering (Men et al. 2023).

However, further systematic analysis has found that there are few targets for rational transformation in the core pathways. Compared to rational genetic engineering focusing on core synthetic pathways, the randomness of mutation breeding is more advantageous and feasible for performance improvement with unknown mechanisms, such as increasing fermentation robustness, mycelium morphology, and stress resistance, and optimising the underlying metabolic network (Xi et al. 2023). In addition, mutation breeding can effectively improve the complex metabolic networks associated with core synthetic pathways, which is difficult to achieve with rational genetic modification. Efficient parental strain with excellent basal metabolic network is also crucial for metabolic engineering of core biosynthetic pathway, which is more conducive to obtaining more efficient engineered strains and towards green biomanufacturing (Su et al. 2024).

Heavy-ion irradiation, as a novel breeding method, has demonstrated high efficiency in creating diverse new mutants (Yanagisawa et al. 2022; Yan et al. 2024). Compared to other physical mutagenic sources, such as X-rays and γ-rays, disparities in both physical and biological effects are readily apparent (Hamada 2009). This method possesses distinct advantages, including strong penetration, extensive sample processing capabilities, and a wide range of mutagenic effects, thereby establishing itself as a highly potent and efficient mutagenic technique (Shikazono et al. 2002; Tanaka et al. 2010). Filamentous fungi are a relatively complex class of multicellular eukaryotic microorganisms that produce a variety of secondary metabolites (Hou et al. 2023; Shi et al. 2024). Although there is little research on the mutagenesis caused by heavy-ion irradiation, many valuable achievements have also been discovered. Hu et al. (2014a, 2014b) increased the citric acid production of *Aspergillus niger* by $^{12}C^{6+}$ ion beam irradiation and successfully achieved technology transfer with the enterprise. Li et al. (2011) used 80 MeV/n $^{12}C^{6+}$ ion beam irradiation to produce the lipid-lowering drug lovastatin and screened for a mutant of *Aspergillus terreus* CA99, whose production increased fourfold. It can be seen that heavy-ion irradiation has a good application effect in the breeding of filamentous fungi.

To date, there have been no reports of utilising heavy-ion irradiation to produce high-yield mutants of FR901379 in *C. empetri*. In this work, FR901379 production strains with better fermentation performance were selected through heavy-ion irradiation and efficient screening methods. Meanwhile, the regularity and uniqueness of heavy-ion irradiation damage repair in *C. empetri* were explored on the molecular level. Moreover, associations between mutation sites, genes, and production traits were

analysed via omics, and key genes related to high yield were predicted. This provides theoretical guidance for further metabolic engineering to construct more efficient FR901379-producing strains.

2. Materials and methods

2.1. Microorganism, medium, and cultivation conditions

Coleophoma empetri MEFC09 and *C. empetri* MEFC09-Δ*ku80* were the parent strains used in this study, which were previously stored at our laboratory (Men et al. 2021). These strains demonstrated a FR901379 titre of approximately 0.2–0.3 g/L in shake-flask fermentation. The solid medium potato dextrose agar (PDA), seed culture medium (MKS: soluble starch 15 g/L, sucrose 10 g/L, cotton seed meal 5 g/L, peptone 10 g/L, KH_2PO_4 1 g/L, $CaCO_3$ 2 g/L, and pH 6.5), fermentation medium (MKF: glucose 10 g/L, corn starch 30 g/L, peptone 10 g/L, $(NH_4)_2SO_4$ 6 g/L, KH_2PO_4 1 g/L, $FeSO_4$ 0.3 g/L, $ZnSO_4$ 0.01 g/L, $CaCO_3$ 2 g/L, and pH 6.5), and cultivation conditions were described in the previous study (Men et al. 2021). *Candida albicans* CMCC-(F) 98001 was purchased from National Center for Medical Culture Collections (CMCC).

2.2. Heavy-ion-beam irradiation

Coleophoma empeteri strain MEFC09 and MEFC09-Δ*ku80* were cultured for 8 d at 25 °C on PDA. Subsequently, spores were collected by adding 1 mL of sterile water and agitating the surface with a brush to facilitate spore release. The spore suspension was then filtered through a sterile cloth in a funnel and diluted to 1×10^8 CFU/mL. Subsequently, 1 mL of the spore suspension was transferred into individual 35 mm petri dishes. The dishes were exposed to $^{12}C^{6+}$ ion beam (energy: 80 MeV/u, LET: 40 keV/μm) at the Heavy-Ion Research Facility in Lanzhou (HIRFL) (Yan et al. 2024). The irradiating doses of MEFC09 and Z40-23 were 40, 80, 100, 120, 140, 160, 200, 500, and 800 Gy, respectively, while the irradiating doses of MEFC09-Δ*ku80* were 20, 40, 60, 80, 100, 120, 140, 160, and 200 Gy.

2.3. Detection of the lethality rates

To determine the lethality of *C. empetri* MEFC09 and MEFC09-Δ*ku80* exposed to carbon ions, the spore suspension was coated onto a PDA plate. After 6–8 d of cultivation, the colonies were counted and the mortality rate was calculated. The mortality rate was calculated using the following equations:

$$\text{Lethal rate} = (A\text{-}B)/A \times 100\%$$

Among them, A represents the number of colonies grown on the plate after mutagenesis, and B represents the number of colonies grown on the plate without mutagenesis. The data were from single experiments.

2.4. Screening of the mutants for FR901379 production

Following irradiation, spore suspensions of *C. empeteri* (10^8 CFU/mL) treated with mutagens and untreated controls were plated on PDA plates. The plates were then incubated at 25 °C for 6 to 8 d. Mutant colonies were selected and grown on new plates for 3 d. Then, the logarithmic growth phase of the *C. albicans* solution was diluted to an OD_{600} of around 0.6 before taking 500 μL and mixing it with 15 mL of soft agar to cover the plate. After 24 h, the diameter of the inhibition zone can be measured, and it will not change over time. Later, the mutants with a large inhibition zone were further evaluated in a 250 mL flask during the second round of screening. Several mutants with the highest concentration of FR901379, obtained through the primary and second-round screening, were further tested for their genetic stability.

2.5. Determination of FR901379 yield

The FR901379 concentration of *C. empetri* MEFC09, *C. empetri* MEFC09-Δ*ku80*, and the mutants were detected according to Men et al. (2021). Briefly, a 1 mL aliquot of the culture was extracted with methanol (5 times volume) using ultrasonic crushing for 1 h. The resulting fermentation broth was centrifuged at 10,000 × *g* for 5 min, and the supernatant was analysed for FR901379 concentration using high-performance liquid chromatography (HPLC) with monitoring at 210 nm.

2.6. Whole-genome re-sequencing

Genomic DNA was extracted using the SDS method (Lim et al. 2016). The extracted DNA underwent

agarose gel electrophoresis for detection and was quantified with a Qubit® 2.0 Fluorometer (Thermo Scientific). Each sample utilised 1 μg of DNA as input material for sample preparation. Sequencing libraries were constructed with the NEBNext® Ultra™ DNA Library Prep Kit for Illumina (NEB, USA) as per the manufacturer's instructions, incorporating index codes to assign sequences to individual samples. Whole-genome sequencing of *C. empetri* was performed on an Illumina NovaSeq PE150 at Beijing Novogene Bioinformatics Technology Co., Ltd.

2.7. Transcript analysis of the mutant strain

Transcriptomic analysis was performed on selected mutants Z40-23, ZZ-138 and the wild strain MEFC09. Initially, the strains were cultured in 50 mL of seed medium in 250 mL shake flasks at 25 °C and 220 r/min. Then, samples were collected and total RNA was extracted following the protocol outlined in the TRIzol® Reagent manual (Novogene, Beijing, China). The extracted RNA was used for cDNA library construction, which was subsequently sequenced on the Illumina Novaseq 6000 platform. The index of the reference genome and paired-end clean reads were aligned to the reference genome and built using Hisat 2 v2.0.5. Differential expression analysis of two groups was performed using the DESep2 package. The resulting *p*-value was adjusted using Benjamini and Hochberg's approach for controlling the false discovery rate.

2.8. Analytical methods

Clean reads were generated by filtering raw reads using Fastp software with default settings. Then, clean reads were mapped to the genome using Bowtie2. The generated bam file was used for the detection of the individual SNP (single nucleotide polymorphism) and InDel (insertion and deletion) of small fragments (<50 bp) using SAMtools. All SNP/InDel sites were annotated by ANNOVAR tool. SV (structural variation) between the reference and the sample was identified by BreakDancer software (V1.4.4, http://breakdancer.sourceforge.net/) (Chen et al. 2009). CNVs (copy-number variations) between the reference and the sample were screened by CNVnator software (v0.3, http://sv.gersteinlab.org/) (Abyzov et al. 2011). The variation map of the whole genome was created by TBtools to show coverage and the distribution of SNP and InDel information (Krzywinski et al. 2009).

2.9. Statistical analysis

All experiments were conducted in triplicates unless otherwise specified. The data plotted in the graphs represent the mean values of the replicates with the corresponding standard deviations. Statistical significance was assessed using a t-test, with differences deemed significant at a p-value <0.05.

3. Results and discussion

3.1. Establishment of high-throughput screening methods

In addition to efficient mutation breeding methods and high-quality mutation libraries, high-throughput screening is another important factor in determining the success or failure of strain mutagenesis (Liu et al. 2017). In order to quickly screen high-yielding strains, a high-throughput screening method for the preliminary screening of *C. empetri* was established based on the size of inhibition zone (Figure 1). Firstly, monoclones cultured on agar plates were selected and transferred onto fresh agar plates for 3-day subculture. This will prevent leakage during screening, as colonies distributed on the agar plate are in an ideal state, often with many colonies close together or connected. Subsequently, *C. albicans* suspension in the logarithmic growth phase was taken and mixed into soft agar to cover the plate instead of spraying the *C. albicans* with a sprayer, which would reduce errors and prevent contamination. Furthermore, *C. albicans* is an opportunistic pathogen, so covering them instead of spraying will be safer. After covering the Petri dish, the diameter of the inhibition zone can be measured after 24 h, and it did not change as time passed. Finally, strains with large inhibition zone were selected and sent for re-screening through shake flask fermentation.

3.2. Lethal effects of the $^{12}C^{6+}$ ion beam on MEFC09 and MEFC09-Δku80

DNA double-strand breaks (DSBs) are a critical primary form of damage, commonly induced by heavy-ion

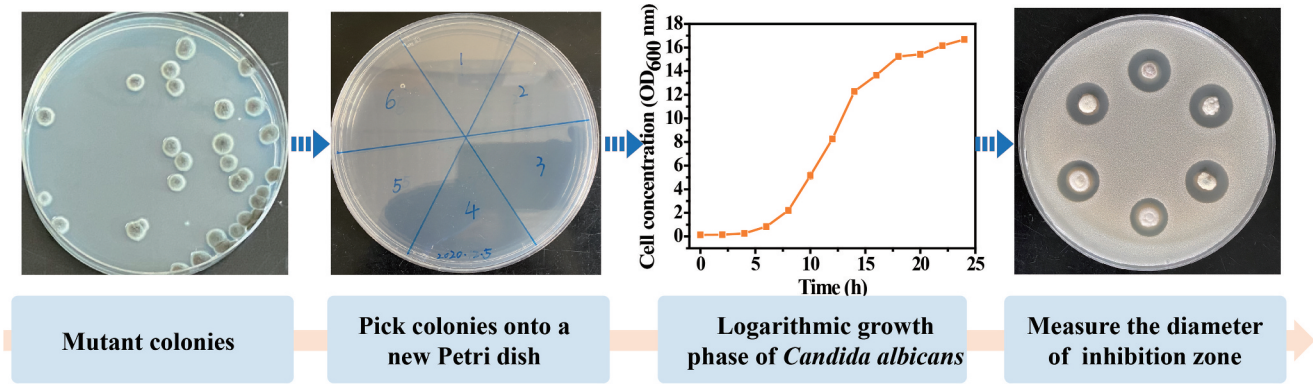

Figure 1. High throughput screening flowchart.

irradiation (Averbeck et al. 2016). In eukaryotic cells, DSBs are primarily repaired through two pathways: nonhomologous end-joining (NHEJ) and homologous recombination (HR) (Ma et al. 2013). In filamentous fungi, the NHEJ pathway occupies a dominant position in repair. Deleting the genes of *ku70*, *ku80*, or *ligD* could inactivate the NHEJ pathway, making the HR pathway dominant (Ninomiya et al. 2004; Huang et al. 2016). We selected different doses of $^{12}C^{6+}$ ion radiation to induce mutations in wild-type strain MEFC09 and the NHEJ-defective strain MEFC09-*Δku80*. The results showed that the MEFC09 strain had a fatality rate of only 32.8% at 40 Gy, which increased to 83.6% at 100 Gy, and reached 100% at 800 Gy (Figure 2a). In contrast, the MEFC09-*Δku80* strain had a fatality rate of 95% at 20 Gy, and a fatality rate of 97% at 40 Gy (Figure 2b). This indicates that the NHEJ-defective strain is more sensitive to heavy-ion radiation, resulting in higher fatality rates at the same radiation dose.

Additionally, the fatality rates of the two strains exhibit a "saddle-shaped" relationship with the irradiation dose of $^{12}C^{6+}$ ion beam. This differs from the conventional "shoulder type" or "straight" survival curves commonly observed in traditional irradiation methods applied to living organisms, such as exposure to ultraviolet or gamma rays (Hu et al. 2018). The phenomenon is characterised by a rapid escalation in cell damage and viability reduction as radiation dosage rises during the initial mortality rate upsurge phase. Subsequently, as the dosage reaches a threshold, unclear cellular repair mechanisms are triggered, elevating cell survival rates. However, at higher dosage levels, the damage from radiation becomes irreversible, resulting in a further decline in survival rates (Ning and Long 2009).

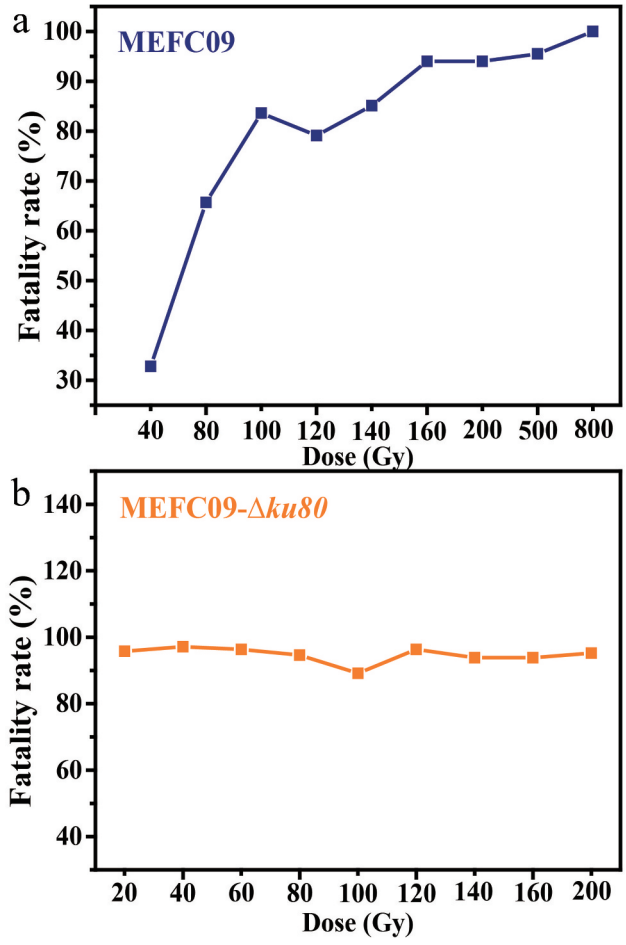

Figure 2. The lethal rate curve of *Coleophoma empetri*. (a) The effect of $^{12}C^{6+}$ ions doses on lethality rate of *C. empetri* MEFC09. (b) The effect of $^{12}C^{6+}$ ions doses on lethality rate of *C. empetri* MEFC09-*Δku80*.

3.3. The first-round mutagenesis and screening mutants

After irradiation, a high-throughput screening method was used to identify high-yield mutants. This process involved primary screening utilising the inhibition zone

and secondary screening based on fermentation. For primary screening, 64 monoclones were selected from approximately 258 clones based on the measurement of inhibition zone, using irradiation with different doses of $^{12}C^{6+}$ ion beam. During the secondary screening, ten mutants (Z40-1, Z40-5, Z40-6, Z40-12, Z40-13, Z40-16, Z40-23, Z80-12, Z120-5, Z120-6) showed higher FR901379 titre compared to the wild-type MEFC09 at 40 Gy, 80 Gy, and 120 Gy. Especially, the titre of FR901379 reached 0.73 g/L in the mutant Z40-23, which was 3.7 times higher than *C. empetri* MEFC09 ($p < 0.0001$) (Figure 3a).

In addition, the 10 mutants exhibited smaller, darker, and more compact colony morphology (Figure 3c). This observation aligns with previous research showing a reduction in colony size with an increased concentration of FR901379 in *C. empeteri* F-11899 following UV mutagenesis (Kanda et al. 2009). Meanwhile, the mycelium pellets in the mutant fermentation broth appeared

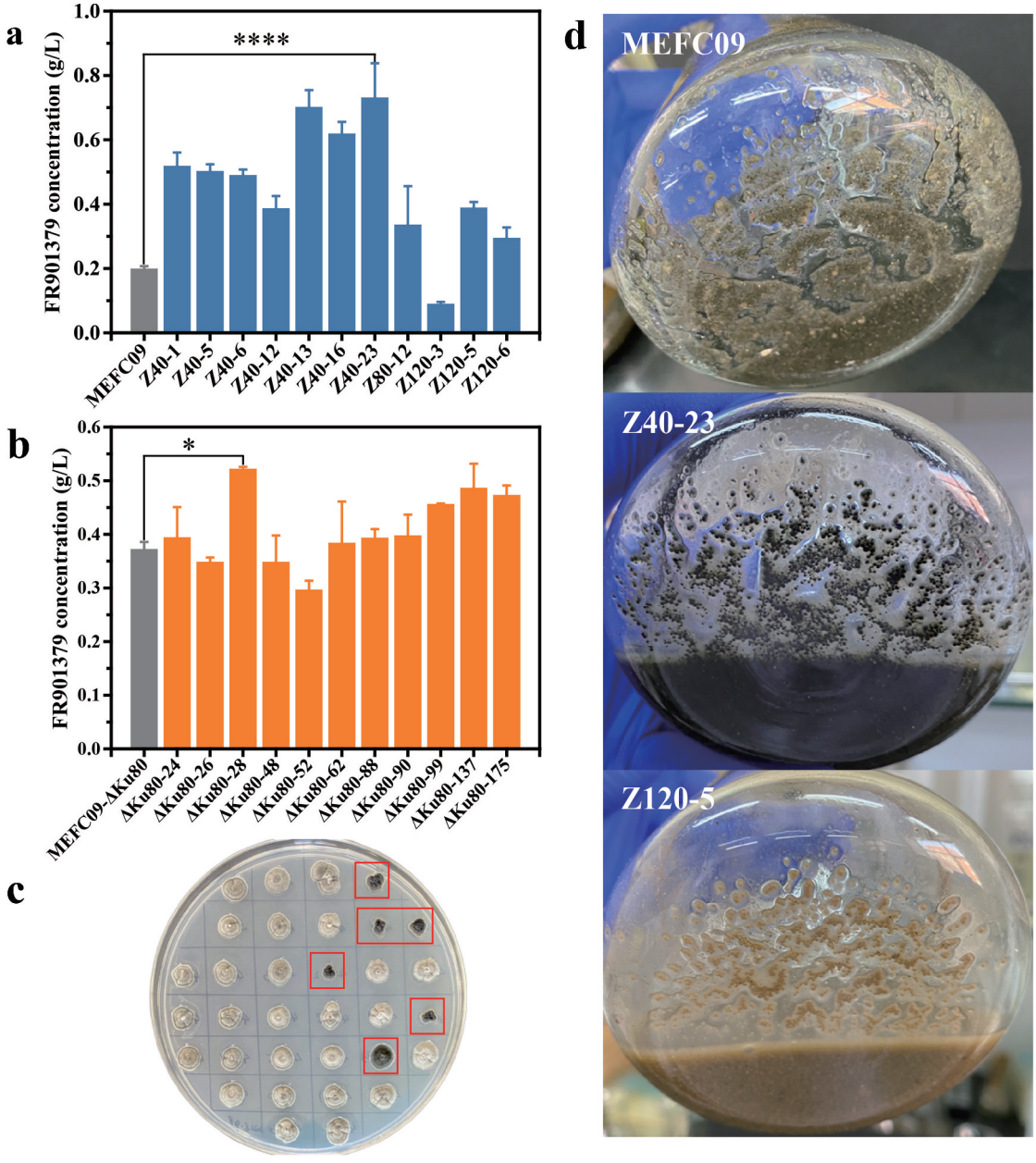

Figure 3. The screening of mutants for FR901379. (a) Effects of $^{12}C^{6+}$ ions on the FR901379 production of *Coleophoma empetri* MEFC09. (b) Effects of $^{12}C^{6+}$ ions on the FR901379 production of *C. empetri* MEFC09-Δ*ku80*. (c) Changes in morphological differentiation of FR901379 high-yield strains obtained from MEFC09 after $^{12}C^{6+}$ ion irradiation. (d) Changes in fermentation status of FR901379 high-yield strains obtained from MEFC09 after $^{12}C^{6+}$ ion irradiation.

more uniform and less viscous compared to the wild-type strain (Figure 3d). In the fermentation process of filamentous fungi, mycelium morphology plays a crucial role in metabolite production (Niu et al. 2020). Figures 3c,d demonstrated that the morphology and size of mycelium may correlate with the FR901379 titre, with smaller mycelium pellets being favoured for FR901379 production.

Furthermore, to evaluate the impact of NHEJ-deficient strains as irradiated materials on the diversity of mutagenesis libraries, mutants were selected from the irradiated MEFC09-Δ*ku80* mutant library. As shown in Figure 3b, a total of 59 monoclonal clones were selected from around 325 clones based on the measurement of inhibition zone diameter. However, only a limited number of high-yield strains were obtained through fermentation. Notably, the increase in FR901379 production was not particularly significant, with the highest observed in the *Δku80*-28 strain at 0.52 g/L, which increased by about 40.3% compared to the control strain *C. empetri* MEFC09-Δ*ku80* ($p < 0.05$).

3.4. MEFC09-Δku80 showed a higher mutation frequency after irradiation with the $^{12}C^{6+}$ ion beam

The characteristics of DNA damage generated by different mutation sources are significantly different. Different organisms also have differences in DNA damage repair mechanisms, leading to unique mutations (Bajinskis et al. 2012; Averbeck et al. 2016). Ionizing radiation results in various forms of DNA damage, such as apyrimidinic sites (APs), single-strand breaks (SSBs), double-strand breaks (DSBs), and DNA-protein cross-links. Double-strand breaks (DSBs) are particularly significant as they can cause genome rearrangement, mutations, and even cell death, making them critical DNA lesions (Dianov et al. 2001; Averbeck et al. 2016). Heavy-ion beams are well known for their significant impact on cellular components, particularly for inducing DSBs. To gain insight into the mutagenic effect of heavy-ion beams, the wild-type strain MEFC09 and the NHEJ-defective strain MEFC09-Δ*ku80* were irradiated with $^{12}C^{6+}$ ion beam, and the type of mutations generated in the survivors was re-sequenced and analysed.

The results revealed that the total number of mutations in the MEFC09-Δ*ku80* mutant group was higher than in the MEFC09 mutant group. Specifically, the MEFC09-Δ*ku80* group showed a range of 3,670 to 4,457 for InDels and 1,406 to 1,506 for SNPs, while the MEFC09 group had a range of 3,148 to 4,085 for InDels and 1,494 to 1,531 for SNPs. This suggests an increase of InDels and SNPs in NHEJ-defective mutants compared to MEFC09 mutants ($p = 0.0001$). In the MEFC09 mutant group, the number of SVs remained in the single digits, contrasted with the MEFC09-Δ*ku80* mutant group where the count of SVs varied from tens to hundreds (Figure 4a, Table S1). And it was also higher than that in the MEFC09 mutant group ($p = 0.0001$). The results align with our expectations as the wild-type strain MEFC09 possesses two DNA repair pathways: NHEJ and HR, while the MEFC09-Δ*ku80* strain only has the HR repair pathway. After mutagenesis, the repair capacity of the MEFC09-Δ*ku80* was weakened, resulting in a higher incidence of InDels, SNPs, and SVs. Additionally, the single-nucleotide mutations in the MEFC09 mutant group and the MEFC09-Δ*ku80* mutant group were compared, it was found that 85% of the mutations were the same. The MEFC09 mutant group had only 30 unique mutations, while the MEFC09-Δ*ku80* mutant group had 801 unique mutations (Figure 4c). Theoretically, 801 unique mutations in the MEFC09-Δ*ku80* mutant group should be repaired through the HR pathway. However, enrichment analysis revealed that 99% of the mutations are located in intergenic regions and non-coding regions, and these mutations are relatively scattered (Figure 4d).

In addition, a series of pieces of evidence reveals that high-LET radiation induces the occurrence of two or more damages within 1–2 helical turns of DNA (~10 nm), a dense form of damage known as DNA cluster damage (MDS) (Brenner and Ward 1992). MDS is more difficult to repair than individual DSBs, and it may even be irreparable in some cases (Okayasu et al. 2006; Lorat et al. 2016). This is a main reason why high-LET radiation has higher biological effects than low LET-radiation (Oike et al. 2016; Schipler et al. 2016). In our study, two or more mutations within 20 bp were identified as an MDS site in two mutant groups, respectively. The results revealed that the number of MDS in the MEFC09 mutant group was 842–1,075, while in the MEFC09-Δ*ku80* mutant group was 1,053–1,202 (Figure 4b, Table S2). It indicates that the weaker repair ability of the MEFC09-Δ*ku80* strain, resulted in an increase in the number of MDS ($p = 0.0001$).

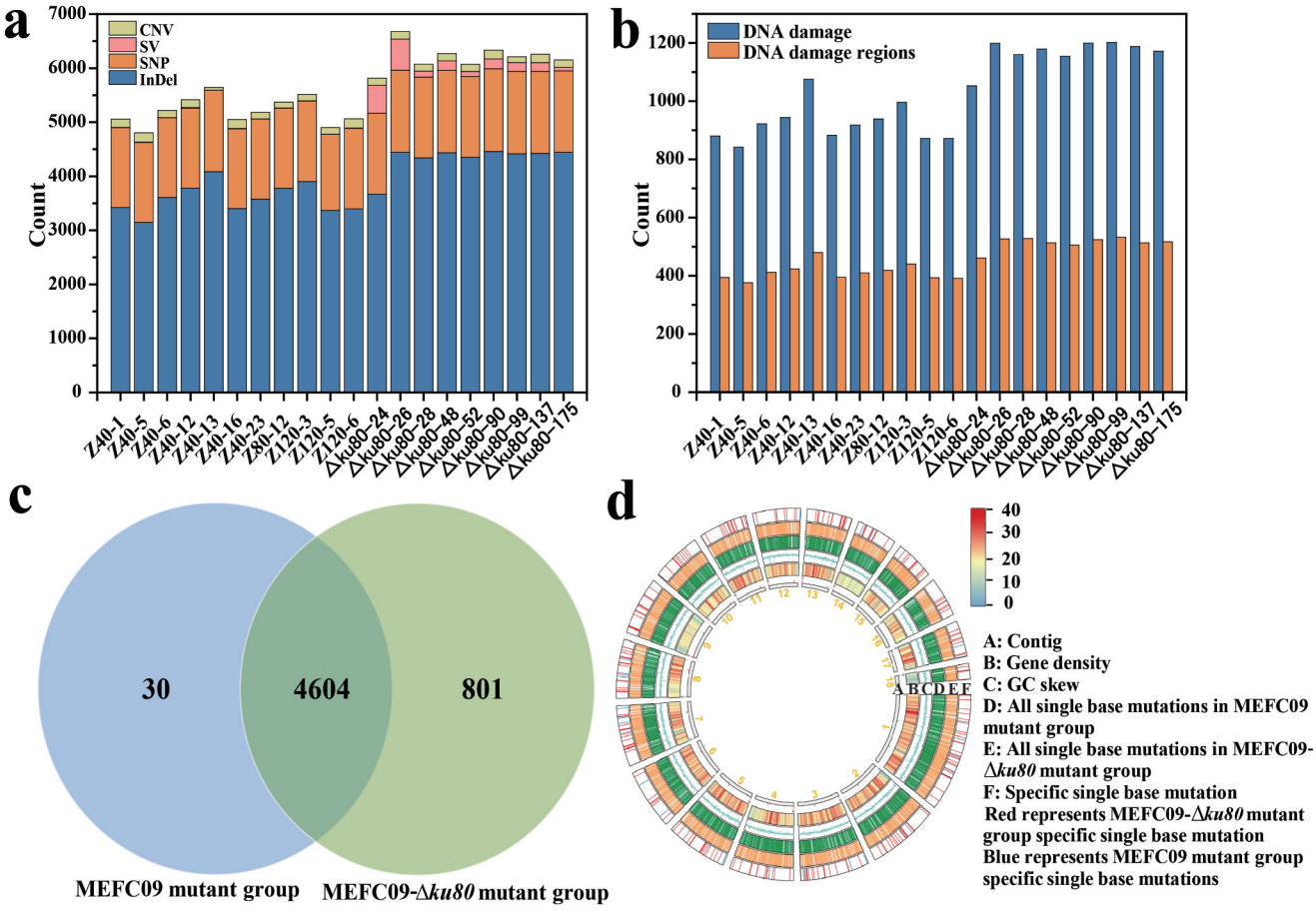

Figure 4. Mutation analysis between MEFC09 mutation group and MEFC09-Δ*ku80* mutation group. (a) The statistics of mutations in mutant strains. (b) The total number of MDS in mutant strains. (c) The Venn diagram of specific single nucleotide mutations for two groups. (d) The enrichment analysis of specific single base mutation sites for two groups.

3.5. The second-round mutagenesis and screening high-yielding mutants

For further enhancement of the FR901379 titre, a second round of mutagenesis was conducted with *C. empeteri* Z40-23 as the initial strain. The outcomes revealed that the viability rates of Z40-23 continued to display a characteristic "saddle-shaped" pattern (Figure 5a) (Ning and Long 2009). Ninety-one clones were selected and transferred into shake flasks based on their order of appearance on agar plates and the diameter of the inhibition zone for fermentation evaluation. The titres of FR901379 showed a significant increase in three mutants, particularly in the ZZ-138 mutant, where the titre reached 1.12 g/L. This amount was 56.7% and 253.7% higher than the titres in *C. empetri* Z40-23 and MEFC09, respectively ($p < 0.0001$) (Figure 5b). By comparing the colony morphology of MEFC09 to Z40-23 and ZZ-138 mutants, it was found that Z40-23 mutant grew darker, smaller, and more robust than MEFC09, while the ZZ-138 mutant was smaller and appeared whiter than the Z40-23 mutant (Figure 5c). The decreased colony size with increasing concentration of FR901379 suggested that the heavy-ion irradiation mutagenesis altered the colony morphology of the mutants, making it more beneficial to synthesise FR901379 (Kanda et al. 2009).

Meanwhile, we also compared the growth rates of the three mutants and no differences were observed between MEFC09, Z40-23, and ZZ-138 (Figure 5c). Significant differences were noted in the state of the fermentation broth among MEFC09, Z40-23, and ZZ-138. Specifically, the fermentation broth of Z40-23 and ZZ-138 exhibited lower viscosity, characterised by smaller and more uniform mycelium pellets compared to those of MEFC09 (Figure 5d). The viscosity of the fermentation broth and mycelial morphology are crucial factors influencing the metabolism of

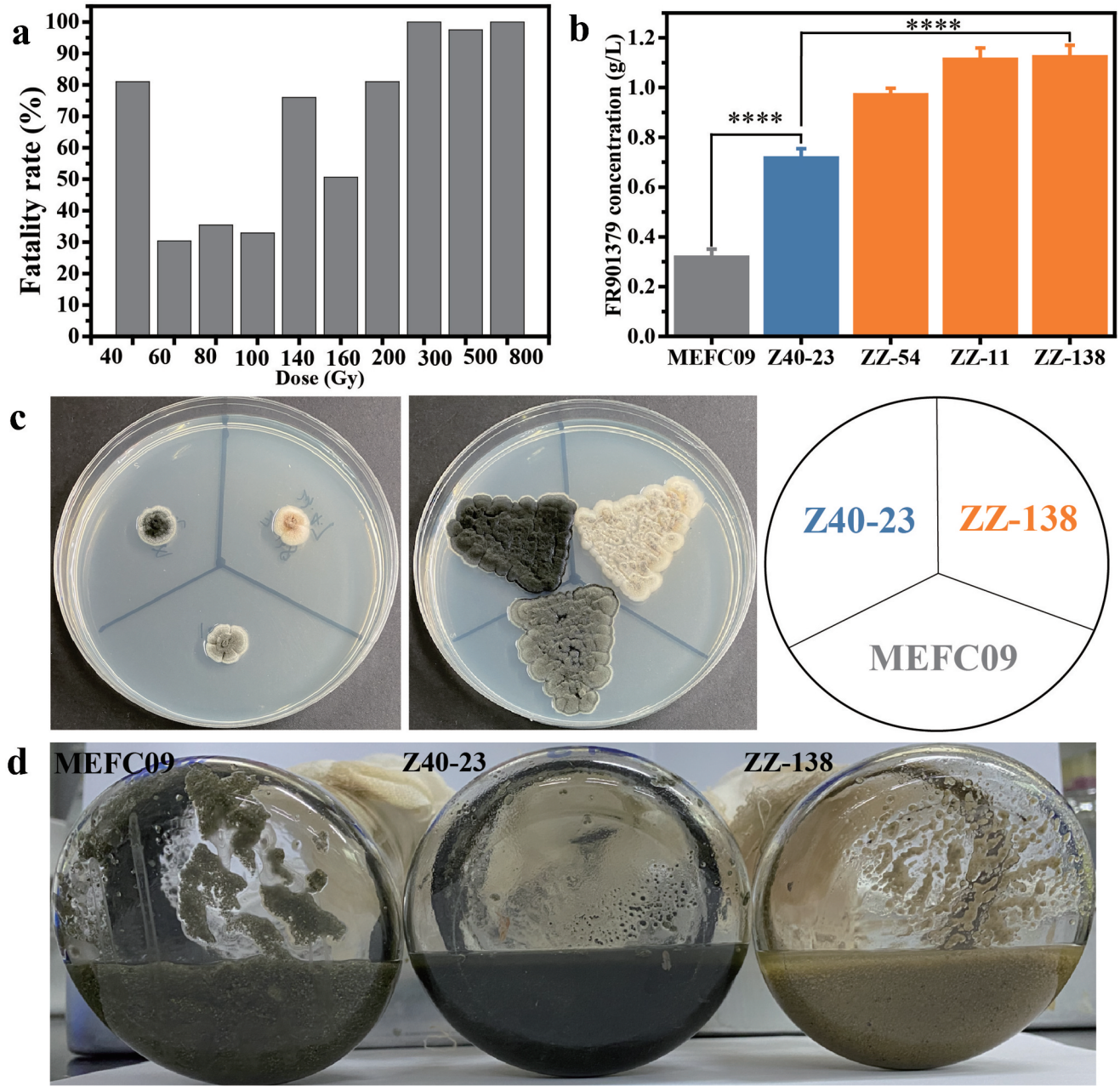

Figure 5. FR901379 production and morphological differentiation of the mutants in the second-round mutagenesis compared with the WT and Z40-23 mutant. (a) The effect of $^{12}C^{6+}$ ions doses on lethality rate of *Coleophoma empetri* Z40-23. (b) FR901379 titers were quantified after the second-round mutagenesis. (c) Changes in morphological differentiation of FR901379 high-yield strains obtained from MEFC09 after $^{12}C^{6+}$ ion irradiation. (d) Changes in fermentation status of FR901379 high-yield strains obtained from MEFC09 after $^{12}C^{6+}$ ion irradiation.

filamentous microorganisms. Various methods have been documented to regulate both the viscosity of the fermentation broth and mycelial morphology with the aim of enhancing the production of secondary metabolites (Niu et al. 2020). The results showed that the FR901379 titre might be caused by improved mycelial morphogenesis, and lower viscosity of the fermentation broth and regular mycelium pellet were beneficial for improving the FR901379 titre of Z40-23 and ZZ-138 (Men et al. 2023). We demonstrated that heavy-ion beam irradiation had a prominent mutagenic effect on *C. empetri* and strongly improved the titre of FR901379. These findings suggest that it is a feasible method for the mutation breeding of FR901379 production of *C. empetri*.

3.6. Omics analysis of high-yield mutants

The above elaborations highlighted the optimal mutants displaying superior phenotypes and high FR901379 production capacity, indicating their potential as valuable candidates in the micafungin industry. Yet, it is imperative to analyse the genomic variations linked to phenotypes and FR901379 synthesis to delve deeper into the molecular mechanisms of metabolic regulation in superior mutants derived via heavy-ion irradiation mutagenesis. Ten high-yield strains from the MEFC09 mutant group and the wild type (WT) were designated as the experimental and control groups, respectively. Compared with WT, it was found that 71% and 58% of the genes related to InDel and SNP mutation sites among the 10 strains in the functional region were the same, respectively (Table S3, Table S4). In addition to putative and unidentified proteins, the proteins produced by these genes primarily consist of oxidoreductases, transporters, kinases, and methyltransferases. Oxidoreductases (A04734, A04841, A06768, A08992, A00981, A05711, A08062, A03619, A08967, A02460, A03231, A05592, A06810) like cytochrome P450 enzymes play an important role in the biosynthesis of natural fungal products due to their wide substrate range, strong catalytic multifunctionality, and high participation frequency (Zhang et al. 2021). Besides oxidoreductases, some mutant genes related to membrane proteins were also found, such as A00035, A01236, A03266, A07050, A04547, A09177, A02623, and A02229. Membrane proteins play diverse and essential roles in various life processes of organisms, such as cell proliferation and differentiation, energy conversion, signal transduction, and molecular transport (Santos et al. 2017). In addition, four mutations are related to transferase (A00181, A02506, A08274, A08274), which play an important role in the morphology and physiological metabolism of fungi (Shi et al. 2021). It was reported that by knocking out the methyltransferase gene *Rmtc* in *Penicillium expansum*, the spore production decreased, the germination of conidia slowed down, and fungal pigment synthesis was inhibited (Xu et al. 2021). This suggested that $^{12}C^{6+}$ ion irradiation mutagenesis most likely generated mutations in genes that encode key enzymes involved in morphological differentiation, leading to the growth of high-yield strains with small black morphology.

Interestingly, four mutations encoding protein kinases (A04529, A06461, A07756, A08146) were also found. In eukaryotes, protein kinases are involved in signal transduction, cellular metabolism, and so on (Leipheimer et al. 2019; Zhang et al. 2020). The two-component regulatory systems, comprising sensor kinase and response regulator proteins, play a crucial role as a vital regulatory factor responsible for modulating physiological metabolic processes like cell growth, differentiation, and metabolism. These systems are particularly integral to morphological differentiation and the synthesis of secondary metabolites in *Streptomyces* (Mendes et al. 2007). Additionally, mutations are related to zinc finger transcription regulatory factor (A01830, A09288, A09969), translation initiation factor (A06689, A06953), transcription initiation factor (A01931) and the ribosome (A00472) were found. It was reported that Zn(II)-Cys(6) is a class of zinc finger transcription factors that only exist in fungi, and these transcription factors can affect the growth and developmental phenotype of strains (Carrillo et al. 2017; Gong et al. 2024). Protein biosynthesis involves four steps: initiation, extension, termination, and ribosomal cycle, and these genes are closely related to protein synthesis (Beznosková et al. 2013; Tseng et al. 2022). The results above suggested that the mutations in the genes encoding morphological differentiation might improve the production of FR901379, which is consistent with the results of Figures 3 and 5.

DNA sequencing analysis revealed that compared to γ-irradiation, heavy-ion irradiation mutagenesis is more likely to cause CNV and SV deletions (Masumura et al. 2002; Yatagai et al. 2002). To explore the deeper insight into how the heavy-ion irradiation leads to higher FR901379 titre in mutants compared to WT, the CNV and SV mutations of mutants were analysed. In the present study, if a CNV occurred in more than half of the samples within a group, it was designated as group-shared CNV. A total of 102 and 133 group-shared CNVs were identified in the high-yield strains of MEFC09 mutation group and MEFC09-Δ*ku80* mutation group, respectively. Most of them occurred in intergenic regions, with only 8 and 12 genes being affected in the coding regions, among which 6 genes overlapped between the two groups (Figure 6a). Interestingly, four of the genes encode proteins containing the WD40 domain (Figure 6b). Proteins with WD40 repeat sequences play significant roles in

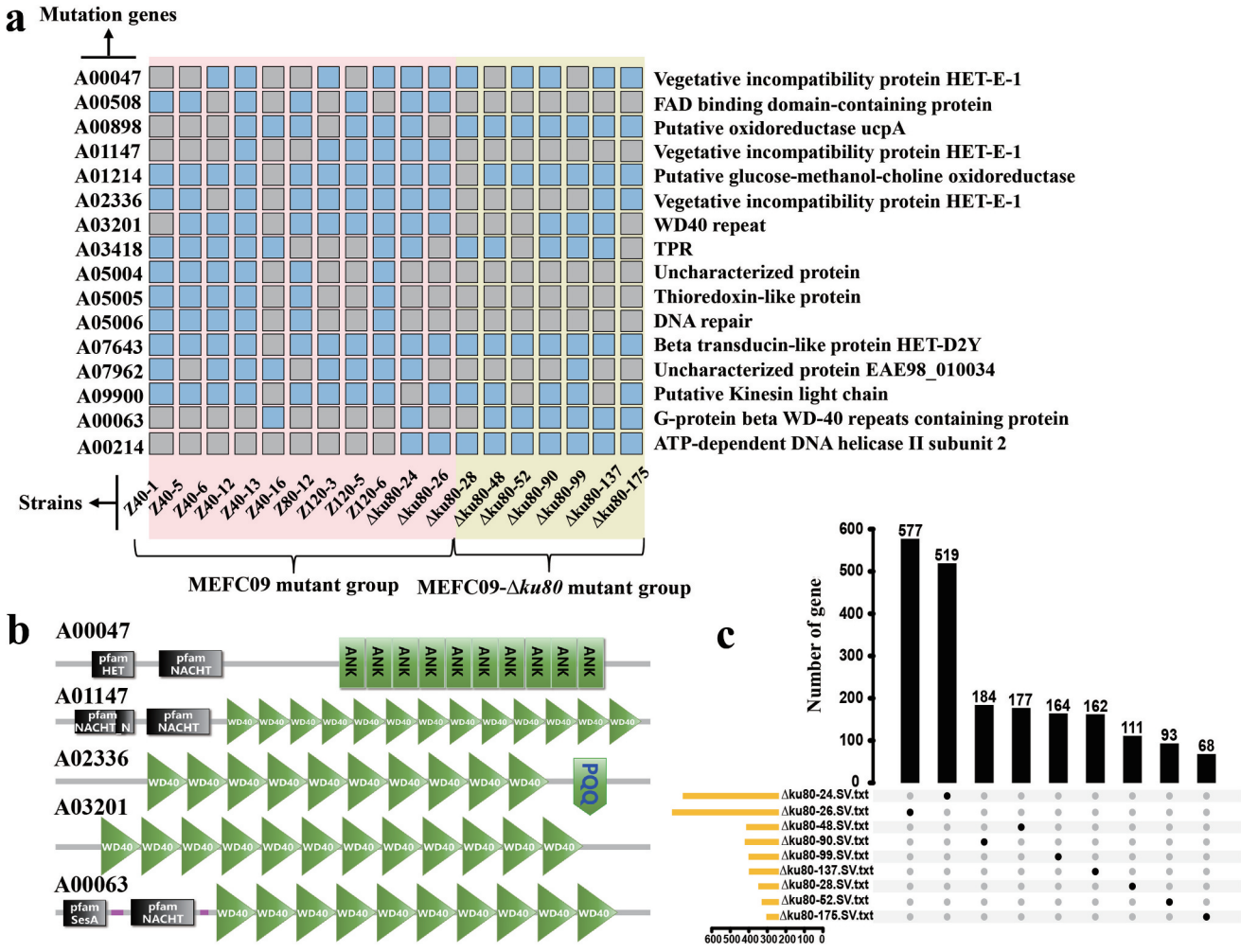

Figure 6. Comparison of CNV and SV mutation genes. (a) Enrichment analysis of CNV mutation genes in the coding region of *Coleophoma empetri* MEFC09 mutant group and MEFC09-Δ*ku80* mutant group. ▯: CNV mutation. ▯: No CNV mutation. (b) Prediction of protein domains encoded by cnv-mutated genes. (c) Enrichment of SV in the MEFC09-Δ*ku80* mutant group.

growth, cell cycle regulation, development, and virulence in lower eukaryotes. Conversely, in higher organisms, they are essential for diverse cellular functions including signal transduction, intracellular transport, development, transcriptional regulation, and immune response (Jain and Pandey 2018). The four genes are considered to be candidate objects for our further studies because they may be associated with the production of FR901379 and the morphological differentiation of mutants. Unfortunately, the SV mutations were relatively random, and no specific pattern has been identified, since no overlapped SVs were found in all samples of the high-yield strains (Figure 6c). These SVs did not affect the synthesis of FR901379, which indicates that SVs caused genomic shrinkage, and may enhance the synthesis efficiency of intracellular FR901379.

Furthermore, a comparative transcriptome analysis was conducted using the wild strain MEFC09 to investigate the potential high-yield mechanism underlying FR901379 biosynthesis in Z40-23 and ZZ-138. The analysis focused on the transcriptional response of various genes within the mcf cluster crucial for FR901379 biosynthesis. Results showed an upregulation of the core gene *mcfA* in both Z40-23 and ZZ-138, compared to the wild-type strain MEFC09, while the expression of other genes remained relatively unchanged (Table S5). This suggests that the increase in FR901379 production should be attributed to the upregulation of *mcfA*.

4. Conclusions

Based on the above work, the pattern of the NHEJ and HR pathways in repairing damage from heavy-ion

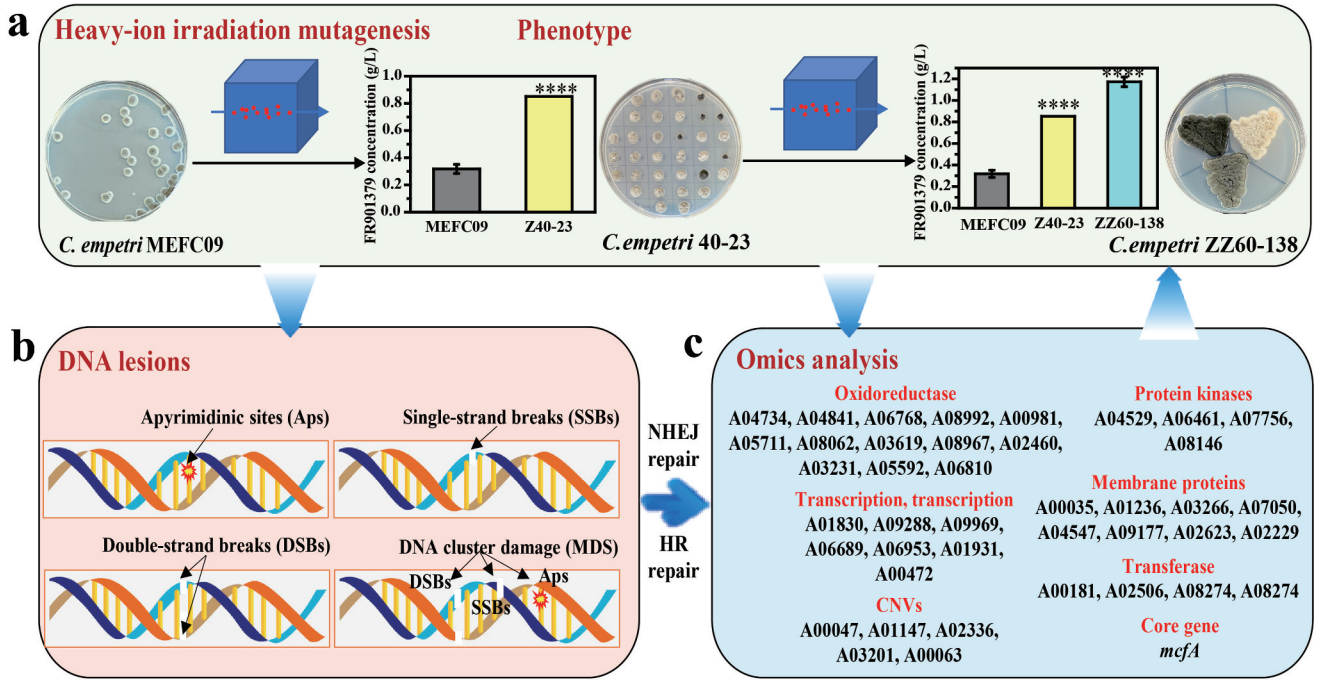

Figure 7. A summary of heavy-ion irradiation damage repair and FR901379 high-yield mechanism in *Coleophoma empetri*. (a) High producing strains of FR901379 were obtained through two rounds of $^{12}C^{6+}$ ion irradiation, which displayed obvious differences in morphology, fermentation, and FR901379 titer. (b) High LET heavy-ion radiation produces dense ionizing radiation. Dense ionizing radiation causes complex DNA lesions, which contain Aps, SSBs, DSBs, and MDS damage within 1–2 helical turns. Then, *C. empetri* initiated different repair mechanisms for repair. (c) In addition, the resequencing results indicated that the majority of InDels, SNPs, and CNVs in the coding region of high-yield mutants were mostly the same. Mutations and large structural deletions of these genes ultimately lead to a significant increase in FR901379 production and morphological differentiation.

irradiation in *C. empetri* and high-yield mechanism of FR901379 was proposed preliminarily (Figure 7). FR901379 high producing strains were obtained through two rounds of $^{12}C^{6+}$ ion irradiation, with a maximum titre of 1.1 g/L, which was enhanced 253.7% than the parent strain. The high-yield mutants displayed obvious differences in morphology, fermentation, and FR901379 titre compared to the parent strain (Figure 7a). Heavy-ion irradiation produces dense ionising radiation, and MEFC09 and MEFC09-Δ*ku80* all generated APs, SSBs, DSBs, and MDSs after $^{12}C^{6+}$ ion irradiation. Then, MEFC09 and MEFC09-Δ*ku80* initiated different repair mechanisms for repair. The MEFC09-Δ*ku80* with a disrupted NHEJ pathway is more sensitive to heavy ion radiation, resulting in higher lethality rates at the same radiation dose, as well as more InDels, SNPs, SVs, and MDS mutations (Figure 7b). Additionally, the resequencing results indicated that the majority of InDels, SNPs, and CNVs in the codon region of high-yield mutants were mostly the same. The proteins encoded by these genes primarily consist of oxidoreductase, membrane proteins, kinase, methyltransferase, transcription, translation regulatory factors, except for putative and unknown proteins (Figure 7c). Comparative genomic analysis demonstrated that $^{12}C^{6+}$ ion irradiation mutagenesis presumably altered the genes of multiple key enzymes in morphological differentiation while enhancing the FR901379 synthesis in the high-yield mutants. The transcriptome results suggested that the increase in FR901379 production should be attributed to the upregulation of *mcfA*. This study not only enhanced the titre of FR901379 in *C. empetri* but also provided excellent chassis cells for metabolic engineering. More importantly, the analysis of high-yield mechanisms offers essential theoretical insights for metabolic engineering aimed at enhancing the production of FR901379. Meanwhile, exploring the rules of heavy-ion irradiation damage repair at the molecular level in filamentous fungi can provide more theoretical support for better utilisation of heavy-ion irradiation mutagenesis.

Disclosure statement

No potential conflict of interest was reported by the author(s).

Funding

This work was supported by National Key R&D Program of China [2021YFC2102600], the National Natural Science Foundation of China [32100049, U2032139, 32300050, 32070056], Key R&D Program of Shandong Province [2021ZDSYS02]. X.L. and X.H. are supported by the Shandong Taishan Scholarship.

Author contributions

X.L. and X.H. conceived the project and supervised the research; X.H. and Y.L. designed the experiments; Y.L., P.M., M.G., W.H., and Z.W. performed the heavy ion radiation experiments; Y.L., B.W., and Y.Z. performed the screening and fermentation experiments; Y.L. and X.Z. performed the resequencing analysis; X.L., M.W., X.H., and Y. L. analysed all data and wrote the manuscript.

References

Abyzov A, Urban AE, Snyder M, Gerstein M. 2011. Cnvnator: an approach to discover, genotype, and characterize typical and atypical CNVs from family and population genome sequencing. Genome Res. 6:974–984. doi: 10.1101/gr.114876.110.

Averbeck NB, Topsch J, Scholz M, Kraft-Weyrather W, Durante M, Taucher-Scholz G. 2016. Efficient rejoining of DNA double-strand breaks despite increased cell-killing effectiveness following spread-out Bragg peak carbon-ion irradiation. Front Oncol. 6:28. doi: 10.3389/fonc.2016.00028.

Bajinskis A, Olsson G, Harms-Ringdahl M. 2012. The indirect effect of radiation reduces the repair fidelity of NHEJ as verified in repair deficient CHO cell lines exposed to different radiation qualities and potassium bromate. Mutat Res. 731(1–2):125–132. doi: 10.1016/j.mrfmmm.2011.12.008.

Beznosková P, Cuchalová L, Wagner S, Shoemaker CJ, Gunišová S, von der Haar T, Valášek LS, Hinnebusch AG. 2013. Translation initiation factors eIF3 and HCR1 control translation termination and stop codon read-through in yeast cells. PLoS Genet. 9(11):e1003962. doi: 10.1371/journal.pgen.1003962.

Brenner DJ, Ward JF. 1992. Constraints on energy deposition and target size of multiply damaged sites associated with DNA double-strand breaks. Int J Radiat Biol. 61(6):737–748. doi: 10.1080/09553009214551591.

Carrillo AJ, Schacht P, Cabrera IE, Blahut J, Prudhomme L, Dietrich S, Bekman T, Mei J, Carrera C, Chen V, et al. 2017. Functional profiling of transcription factor genes in *Neurospora crassa*. G3 (Bethesda). 7(9):2945–2956. doi: 10.1534/g3.117.043331.

Chen K, Wallis JW, McLellan MD, Larson DE, Kalicki JM, Pohl CS, McGrath SD, Wendl MC, Zhang Q, Locke DP, et al. 2009. BreakDancer: an algorithm for high-resolution mapping of genomic structural variation. Nat Methods. 6(9):677–681. doi: 10.1038/nmeth.1363.

Denning DW. 2003. Echinocandin antifungal drugs. Lancet. 362 (9390):1142–1151. doi: 10.1016/S0140-6736(03)14472-8.

Dianov GL, O'Neill P, Goodhead DT. 2001. Securing genome stability by orchestrating DNA repair: removal of radiation-induced clustered lesions in DNA. Bioessays. 23 (8):745–749. doi: 10.1002/bies.1104.

Emri T, Majoros L, Tóth V, Pócsi I. 2013. Echinocandins: production and applications. Appl Microbiol Biotechnol. 97 (8):3267–3284. doi: 10.1007/s00253-013-4761-9.

Gong X, Zhang H, Cheng W, He Z, Ma T, Chen T, Sun Y. 2024. *Aspergillus fumigatus ctf1*–a novel zinc finger transcription factor involved in azole resistance. Mycology. 1–14. doi: 10.1080/21501203.2024.2342521.

Hamada N. 2009. Recent insights into the biological action of heavy-ion radiation. J Radiat Res. 50(1):1–9. doi: 10.1269/jrr.08070.

Hashimoto S. 2009. Micafungin: a sulfated echinocandin. J Antibiot (Tokyo). 62(1):27–35. doi: 10.1038/ja.2008.3.

Hou H, Huang X, Du Z, Guo J, Wang M, Xu G, Geng C, Zhang Y, Wang Q, Lu X. 2023. Integration of biological synthesis & chemical catalysis: bio-based plasticizer trans-aconitates. Green Carbon. 1(1):20–32. doi : 10 .1016/j.greenca.202.

Hu W, Chen J, Wu Q, Li W, Liu J, Lu D, Wang S. 2018. The mutagenesis of *Lactobacillus Thermophilus* for enhanced L-(+)-lactic acid accumulation induced by heavy ion irradiation. Brazn Arch Biol Techn. 60:e16160337. doi: 10.1590/1678-4324-2016160337.

Hu W, Li W, Chen J, Liu J, Shuyang W, Wang J, Lu D. 2014a. Mutant breeding of *Aspergillus niger* irradiated by $^{12}C^{6+}$ for hyper citric acid. Nucl Sci Tech. 25(2):1–4. doi: 10.13538/j.1001-8042/nst.25.020302.

Hu W, Liu J, Chen JH, Wang SY, Lu D, Wu QH, Li WJ. 2014b. A mutation of *Aspergillus niger* for hyper-production of citric acid from corn meal hydrolysate in a bioreactor. J Zhejiang Univ Sci B. 15(11):1006–1010. doi: 10.1631/jzus.B1400132.

Huang X, Chen M, Li J, Lu X. 2016. Establishing an efficient gene-targeting system in an itaconic-acid producing *Aspergillus terreus* strain. Biotechnol Lett. 38(9):1603–1610. doi: 10.1007/s10529-016-2143-y.

Iwamoto T, Fujie A, Sakamoto K, Tsurumi Y, Shigematsu N, Yamashita M, Hashimoto S, Okuhara M, Kohsaka M. 1994. WF11899A, B and C, novel antifungal lipopeptides. I. Taxonomy, fermentation, isolation and physico-chemical properties. J Antibiot (Tokyo). 47(10):1084–1091. doi: 10.7164/antibiotics.47.1084.

Jain BP, Pandey S. 2018. WD40 repeat proteins: signalling scaffold with diverse functions. Protein J. 37(5):391–406. doi: 10.1007/s10930-018-9785-7.

Kanda M, Tsuboi M, Sakamoto K, Shimizu S, Yamashita M, Honda H. 2009. Improvement of FR901379 production by mutant selection and medium optimization. J Biosci Bioeng. 107(5):530–534. doi: 10.1016/j.jbiosc.2009.01.002.

Krzywinski M, Schein J, Birol I, Connors J, Gascoyne R, Horsman D, Jones SJ, Marra MA. 2009. Circos: an information

aesthetic for comparative genomics. Genome Res. 19 (9):1639–1645. doi: 10.1101/gr.092759.109.

Leipheimer J, Bloom ALM, Panepinto JC. 2019. Protein kinases at the intersection of translation and virulence. Front Cell Infect Microbiol. 9:318. doi: 10.3389/fcimb.2019.00318.

Li SW, Li M, Song HP, Feng JL, Tai XS. 2011. Induction of a high-yield lovastatin mutant of *Aspergillus terreus* by $^{12}C^{6+}$ heavy-ion beam irradiation and the influence of culture conditions on lovastatin production under submerged fermentation. Appl Biochem Biotechnol. 165(3–4):913–925. doi: 10.1007/s12010-011-9308-x.

Lim HJ, Lee EH, Yoon Y, Chua B, Son A. 2016. Portable lysis apparatus for rapid single-step DNA extraction of *Bacillus subtilis*. J Appl Microbiol. 120(2):379–387. doi: 10.1111/jam.13011.

Liu YJ, Chen XS, Zhao JJ, Pan L, Mao ZG. 2017. Development of microtiter plate culture method for rapid screening of ε-Poly-L-Lysine-producing strains. Appl Biochem Biotechnol. 183(4):1209–1223. doi: 10.1007/s12010-017-2493-5.

Lorat Y, Timm S, Jakob B, Taucher-Scholz G, Rübe CE. 2016. Clustered double-strand breaks in heterochromatin perturb DNA repair after high linear energy transfer irradiation. Radiother Oncol. 121(1):154–161. doi: 10.1016/j.radonc.2016.08.028.

Ma L, Kazama Y, Inoue H, Abe T, Hatakeyama S, Tanaka S. 2013. The type of mutations induced by carbon-ion-beam irradiation of the filamentous fungus *Neurospora crassa*. Fungal Biol. 117(4):227–238. doi: 10.1016/j.funbio.2013.01.002.

Masumura K, Kuniya K, Kurobe T, Fukuoka M, Yatagai F, Nohmi T. 2002. Heavy-ion-induced mutations in the gpt delta transgenic mouse: comparison of mutation spectra induced by heavy-ion, X-ray, and gamma-ray radiation. Environ Mol Mutagen. 40(3):207–215. doi: 10.1002/em.10108.

Men P, Geng C, Zhang X, Zhang W, Xie L, Feng D, Du S, Wang M, Huang X, Lu X. 2022. Biosynthesis mechanism, genome mining and artificial construction of echinocandin O-sulfonation. Metab Eng. 74:160–167. doi: 10.1016/j.ymben.2022.10.006.

Men P, Wang M, Li J, Geng C, Huang X, Lu X. 2021. Establishing an efficient genetic manipulation system for sulfated echinocandin producing fungus *Coleophoma empetri*. Front Microbiol. 12:734780. doi: 10.3389/fmicb.2021.734780.

Men P, Zhou Y, Xie L, Zhang X, Zhang W, Huang X, Lu X. 2023. Improving the production of the micafungin precursor FR901379 in an industrial production strain. Microb Cell Fact. 22(1):44. doi: 10.1186/s12934-023-02050-0.

Mendes MV, Tunca S, Antón N, Recio E, Sola-Landa A, Aparicio JF, Martín JF. 2007. The two-component phoR-phoP system of *Streptomyces natalensis*: inactivation or deletion of phoP reduces the negative phosphate regulation of pimaricin biosynthesis. Metab Eng. 9(2):217–227. doi: 10.1016/j.ymben.2006.10.003.

Ning Z, Long Y. 2009. Mutation breeding of β-carotene producing strain B. trispora by low energy ion implantation. Plasma Sci Technol. 11(1):110. doi: 10.1088/1009-0630/11/1/22.

Ninomiya Y, Suzuki K, Ishii C, Inoue H. 2004. Highly efficient gene replacements in *Neurospora* strains deficient for non-homologous end-joining. Proc Natl Acad Sci USA. 101 (33):12248–12253. doi: 10.1073/pnas.0402780101.

Niu K, Wu XP, Hu XL, Zou SP, Hu ZC, Liu ZQ, Zheng YG. 2020. Effects of methyl oleate and microparticle-enhanced cultivation on echinocandin B fermentation titer. Bioprocess Biosyst Eng. 43(11):2009–2015. doi: 10.1007/s00449-020-02389-3.

Oike T, Niimi A, Okonogi N, Murata K, Matsumura A, Noda SE, Kobayashi D, Iwanaga M, Tsuchida K, Kanai T, et al. 2016. Visualization of complex DNA double-strand breaks in a tumor treated with carbon ion radiotherapy. Sci Rep. 6:22275. doi: 10.1038/srep22275.

Okayasu R, Okada M, Okabe A, Noguchi M, Takakura K, Takahashi S. 2006. Repair of DNA damage induced by accelerated heavy ions in mammalian cells proficient and deficient in the non-homologous end-joining pathway. Radiat Res. 165(1):59–67. doi: 10.1667/rr3489.1.

Santos R, Ursu O, Gaulton A, Bento AP, Donadi RS, Bologa CG, Karlsson A, Al-Lazikani B, Hersey A, Oprea TI, et al. 2017. A comprehensive map of molecular drug targets. Nat Rev Drug Discov. 16(1):19–34. doi: 10.1038/nrd.2016.230.

Schipler A, Mladenova V, Soni A, Nikolov V, Saha J, Mladenov E, Iliakis G. 2016. Chromosome thripsis by DNA double strand break clusters causes enhanced cell lethality, chromosomal translocations and 53BP1-recruitment. Nucleic Acids Res. 44 (16):7673–7690. doi: 10.1093/nar/gkw487.

Shi D, Zhang Y, Wang J, Ren W, Zhang J, Mbadianya JI, Zhu Y, Chen C, Ma H. 2021. S-adenosyl-L-homocysteine hydrolase FgSah1 is required for fungal development and virulence in *Fusarium graminearum*. Virulence. 12(1):2171–2185. doi: 10.1080/21505594.2021.1965821.

Shi Y, Ji M, Dong J, Shi D, Wang Y, Liu L, Feng S, Liu L. 2024. New bioactive secondary metabolites from fungi: 2023. Mycology. 15(3):283–321. doi: 10.1080/21501203.2024.2354302.

Shikazono N, Tanaka A, Kitayama S, Watanabe H, Tano S. 2002. LET dependence of lethality in Arabidopsis thaliana irradiated by heavy ions. Radiat Environ Biophys. 41 (2):159–162. doi: 10.1007/s00411-002-0157-4.

Su C, Cai D, Zhang H, Wu Y, Jiang Y, Liu Y, Zhang C, Li C, Qin P, Tan T. 2024. Pilot-scale acetone-butanol-ethanol fermentation from corn stover. Green Carbon. 2(1):81–93. doi: 10.1016/j.greenca.2024.02.004.

Szymański M, Chmielewska S, Czyżewska U, Malinowska M, Tylicki A. 2022. Echinocandins-structure, mechanism of action and use in antifungal therapy. J Enzym Inhib Med Chem. 37(1):876–894. doi: 10.1080/14756366.2022.2050224.

Tanaka A, Shikazono N, Hase Y. 2010. Studies on biological effects of ion beams on lethality, molecular nature of mutation, mutation rate, and spectrum of mutation phenotype for mutation breeding in higher plants. J Radiat Res. 51 (3):223–233. doi: 10.1269/jrr.09143.

Tomishima M, Ohki H, Yamada A, Maki K, Ikeda F. 2008a. Novel echinocandin antifungals. Part 1: novel side-chain analogs of the natural product FR901379. Bioorg Med Chem Lett. 18 (4):1474–1477. doi: 10.1016/j.bmcl.2007.12.062.

Tomishima M, Ohki H, Yamada A, Maki K, Ikeda F. 2008b. Novel echinocandin antifungals. Part 2: optimization of the side chain of the natural product FR901379. Discovery of micafungin. Bioorg Med Chem Lett. 18(9):2886–2890. doi: 10.1016/j.bmcl.2008.03.093.

Tseng YT, Sung YC, Liu CY, Lo KY. 2022. Translation initiation factor eIF4G1 modulates assembly of the polypeptide exit tunnel region in yeast ribosome biogenesis. J Cell Sci. 135 (12):jcs259540. doi: 10.1242/jcs.259540.

Ueda S, Kinoshita M, Tanaka F, Tsuboi M, Shimizu S, Oohata N, Hino M, Yamada M, Isogai Y, Hashimoto S. 2011. Strain selection and scale-up fermentation for FR901379 acylase production by *Streptomyces* sp. no. 6907. J Biosci Bioeng. 112(4):409–414. doi: 10.1016/j.jbiosc.2011.06.002.

Xi Y, Fan F, Zhang X. 2023. Microbial L-malic acid production: history, current progress, and perspectives. Green Carbon. 1 (2):118–132. doi: 10.1016/j.greenca.2023.10.005.

Xu X, Chen Y, Li B, Tian S. 2021. Arginine methyltransferase PeRmtC regulates development and pathogenicity of *Penicillium expansum* via mediating key genes in conidiation and secondary metabolism. J Fungi (Basel). 7(10):807. doi: 10.3390/jof7100807.

Yan Y, Shan W, Zhang C, Wu Y, Xing X, Chen J, Hu W. 2024. Strain engineering of *Bacillus coagulans* with high osmotic pressure tolerance for effective L-lactic acid production from sweet sorghum juice under unsterile conditions. Bioresour Technol. 400:130648. doi: 10.1016/j.biortech.2024.130648.

Yanagisawa M, Asamizu S, Satoh K, Oono Y, Onaka H, Hagiwara D. 2022. Effects of carbon ion beam-induced mutagenesis for the screening of RED production-deficient mutants of *Streptomyces coelicolor* JCM4020. PLoS One. 17 (7):e0270379. doi: 10.1371/journal.pone.0270379.

Yatagai F, Kurobe T, Nohmi T, Masumura K, Tsukada T, Yamaguchi H, Kasai-Eguchi K, Fukunishi N. 2002. Heavy-ion-induced mutations in the *gpt* delta transgenic mouse: effect of *p53* gene knockout. Environ Mol Mutagen. 40 (3):216–225. doi: 10.1002/em.10107.

Zhang F, Huang L, Deng J, Tan C, Geng L, Liao Y, Yuan J, Wang S. 2020. A cell wall integrity-related MAP kinase kinase kinase *AflBck1* is required for growth and virulence in fungus *Aspergillus flavus*. Mol Plant Microbe Interact. 33(4):680–692. doi: 10.1094/MPMI-11-19-0327-R.

Zhang X, Guo J, Cheng F, Li S. 2021. Cytochrome P450 enzymes in fungal natural product biosynthesis. Nat Prod Rep. 38 (6):1072–1099. doi: 10.1039/d1np00004g.